Surface relaxation and the long-time diffusion coefficient in porous media: Periodic geometries

Pabitra N. Sen and Lawrence M. Schwartz
Schlumberger-Doll Research, Old Quarry Road, Ridgefield, Connecticut 06877-4108

Partha P. Mitra
Schlumberger-Doll Research, Old Quarry Road, Ridgefield, Connecticut 06877-4108
and Department of Physics, Harvard University, Cambridge, Massachusetts 02138

Bertrand I. Halperin
Department of Physics, Harvard University, Cambridge, Massachusetts 02138
(Received 16 June 1993; revised manuscript received 24 September 1993)

The macroscopic diffusion coefficient, obtained in an ideal pulsed-field-gradient spin-echo (PFGSE) experiment in the long-time limit, should exactly equal that derived from the electrical conductivity only when the surface relaxivity ρ and surface electrical conductivity vanish. In general, the coefficient derived by PFGSE techniques can be either greater or less than its electrical counterpart, depending on the pore geometry and other factors. Formally, the effect of ρ can be seen from the structure of a perturbation expansion based on the $\rho = 0$ time-dependent solutions of the pore space diffusion problem. In addition, analytic results for periodic structures with partially absorbing boundary conditions and numerical simulations are used to illustrate the differences between the diffusion coefficients for $\rho = 0$ and $\rho \neq 0$. In treating disordered media, our simulations are limited to systems that are not heterogeneous beyond the PFGSE diffusion length scale.

I. INTRODUCTION

This paper is concerned with the influence of surface relaxation on the long-time behavior of the diffusion coefficient in homogeneous porous media. In particular, we compare two different diffusion measurements, pulsed-field-gradient spin-echo (PFGSE) magnetic resonance[1-13] and electrical conduction. The diffusion coefficients measured in these experiments are identical only if reflecting boundary conditions apply in both cases.[6] This will not be the case if there is excess surface conductivity[10] (in the electrical measurement) or enhanced surface relaxivity (in the PFGSE measurement). We study here the influence of surface relaxivity, ρ, in model systems which are not heterogeneous beyond the PFGSE diffusion length scale. Only in such systems can PFGSE experiments be meaningfully compared with truly long range measurements like dc electrical conductivity. We assume, further, that the PFGSE diffusion coefficient is measured under ideal circumstances in which internal field inhomogeneities arising from the susceptibility contrast between grain and fluid are either negligible or can be taken care of by proper pulse sequences.[14]

The formation factor is among the most important geometrical parameters characterizing the tortuosity of porous media:

$$F = \frac{D_0}{\phi D_{\text{eff}}} . \tag{1}$$

Here ϕ denotes the porosity (i.e., the volume fraction associated with the pore space), D_0 is the bulk fluid molecular diffusion coefficient, and D_{eff} is the corresponding coefficient when the fluid is confined within the complex pore geometry with reflecting boundary conditions. A common method of estimating F is by measuring electrical conductivity since electrical conduction and diffusion are related by the Einstein relation. Assuming that the solid phase is electrically inert (i.e., that surface conduction can be neglected) we have

$$F \equiv \frac{\sigma_f}{\sigma} \geq 1 , \tag{2}$$

where σ is the conductivity of the porous medium saturated with a fluid of conductivity σ_f. Physically, F reflects the influence of tortuosity (i.e., of constrictions and direction changes) in the flow paths for electrical current. In addition, F is related to fluid flow,[15] sound velocity,[16] and other properties of interest in porous media.

In practice, the direct electrical measurement of F may be problematic. Often the precise value of σ_f is not known. In addition, Eq. (2) does not hold for systems with charged interfaces (e.g., rocks with clays) where the apparent value of F depends on the parameter σ_f.[10] Accordingly, an alternative method of determining this important geometrical quantity would be quite valuable. Under certain conditions, diffusion measurements based on nuclear magnetic resonance (NMR) provide such an alternative.

PFGSE experiments measure the diffusion of nuclear magnetization which arises, physically, out of the diffusive motion of fluid molecules. The magnetization density can be visualized as the density of an ensemble of ran-

dom walkers moving through the pore space and getting either reflected or absorbed at the pore-grain interface.[6] Physically, the absorption of walkers represents the enhanced relaxation of magnetization associated with paramagnetic impurities at the grain surfaces.[17] Let $\langle r^2(t)\rangle_s$ be the mean square displacement of the walkers surviving to time t. In the presence of surface relaxation, the number of walkers is not conserved, so that their motion is not diffusive in the usual sense. However, PFGSE measurement still provides a time-dependent diffusion coefficient via the operational definition:[6]

$$D(t \mid \rho) \equiv \frac{\langle r^2(t)\rangle_s}{6t} , \tag{3}$$

where $\langle\cdots\rangle_s$ denotes an average taken over only those walkers *surviving* to time t. (In Ref. 6 the notation $\langle r^2(t)\rangle_n$ was used, the subscript n denoting a *normalized* expectation value [see Eq. (8), below].) Thus, in the absence of surface relaxation, we have

$$D_{\text{eff}} \equiv D(t \to \infty \mid \rho = 0) \equiv \frac{\langle r^2(t)\rangle}{6t} = \frac{D_0}{F\phi} . \tag{4}$$

We will see that, in principle, $D(t \mid \rho)$ may be either greater or less than $D(t \to \infty \mid \rho = 0)$.

It should be emphasized that the length scale differences between the electrical and PFGSE measurements vis-à-vis sample heterogeneities may be the most important reason for the differences in measured formation factors in many porous media. In the electrical measurement, the macroscopic fields are constant over the entire sample, while in NMR the longest coarse-graining length is the diffusion distance, $\sim (D_0T_1)^{(1/2)}$, which the walkers can go during their lifetime, $\sim T_1$. This distance is typically 10–100 μm in rocks with $T_1 \sim$ 10–1000 ms. Thus the formation factors measured by these two methods can be meaningfully compared only if this length is larger than any inhomogeneity fluctuations in the rock. Otherwise, these fluctuations may be far more important than the effects of surface relaxivity. Clearly, in macroscopically heterogeneous systems, the NMR signals from different parts of the pore space are roughly independent of each other and the total signal is a sum of contributions coming from each part. In the long-time limit, the longest lived NMR signal will dominate the measurement even though the corresponding effective diffusion coefficient may be totally unrelated to that of the entire sample.

Section II begins with a brief review of the central equations that describe diffusion in the presence of partially absorbing boundary conditions. We then present a series of physical arguments to illustrate the relationship between pore geometry and the long-time behavior of $D(t \mid \rho)$. Section II concludes with the derivation of a formal perturbation theory that allows $D(t \mid \rho)$ to be calculated in terms of the $\rho = 0$ solutions of the diffusion problem in the *same* pore geometry. In Sec. III we evaluate the effects of surface relaxivity on the $t \to \infty$ limit of the diffusion coefficient in periodic unconsolidated structures. In Sec. IV we present the results of numerical simulations for several periodic model geometries and also for one of the simplest disordered porous systems, a dense packing of spherical grains. These simulations allow us to illustrate the important interplay between the pore geometry and the influence of ρ.

II. GENERAL CONSIDERATIONS

A. Basic equations

In PFGSE measurements one studies the wave vector ($\mathbf{k}$) and time (t) dependence of a spin-echo amplitude $M(\mathbf{k},t)$. In this experiment, the dephasing and rephasing of the transverse magnetization are modulated by two hard gradient pulses. [If the running time of the measurement sequence is denoted by τ, the applied magnetic field is changed by an amount $\mathbf{g}\cdot\mathbf{r}f(\tau)$ where $f(\tau) = 0$ except for two short intervals, each of duration δ separated by a time t.] We will be concerned with an idealized limit of the PFGSE measurement in which $\delta \to 0$ and $|\mathbf{g}| \to \infty$ such that the magnitude of the wave vector $\mathbf{k} \equiv \gamma\delta\mathbf{g}$ remains finite (here, γ is the proton gyromagnetic ratio). The measured amplitude is then given by

$$M(\mathbf{k},t) = \frac{1}{V_p}\int d\mathbf{r}d\mathbf{r}'\, G(\mathbf{r},\mathbf{r}',t)e^{-i\mathbf{k}\cdot(\mathbf{r}-\mathbf{r}')} , \tag{5}$$

where V_p is the pore volume and the bulk fluid magnetization decay has been factored out. The diffusion propagator G satisfies the diffusion equation in the interior of the pore space with diffusion constant D_0,

$$\frac{\partial G(\mathbf{r},\mathbf{r}',t)}{\partial t} = D_0\nabla^2 G(\mathbf{r},\mathbf{r}',t), \quad t > 0 , \tag{6a}$$

$$G(\mathbf{r},\mathbf{r}',t = 0^+) = \delta(\mathbf{r}-\mathbf{r}') , \tag{6b}$$

and the boundary condition at the surface Σ with an outward normal $\hat{\mathbf{n}}$ is

$$D_0\hat{\mathbf{n}}\cdot\nabla G(\mathbf{r},\mathbf{r}',t) + \rho G(\mathbf{r},\mathbf{r}',t)\,|_{\mathbf{r}\in\Sigma} = 0 . \tag{7}$$

The measured effective diffusion coefficient is obtained from the normalized average

$$6tD(t \mid \rho) = \langle r^2(t)\rangle_s = \frac{\int(\mathbf{r}-\mathbf{r}')^2 G(\mathbf{r},\mathbf{r}',t)d\mathbf{r}d\mathbf{r}'}{\int G(\mathbf{r},\mathbf{r}',t)d\mathbf{r}d\mathbf{r}'} \tag{8}$$

or, equivalently,

$$D_{\text{eff}}(\rho) = -\lim_{t\to\infty}\left[\frac{1}{t}\lim_{k\to 0}\left\{\frac{\partial}{\partial k^2}\ln M(k,t)\right\}\right] . \tag{9}$$

It is clear from Eq. (8) that $D(t \mid \rho)$ is a ratio of two quantities, each of which is influenced by ρ. Both the denominator and numerator decrease as ρ is turned on, reflecting the fact that the average involves only the surviving walkers. We will see, however, that the ratio may either increase or decrease with ρ and that the net behavior of $D(t \mid \rho)$ is not easily predicted.

B. Physical arguments

To develop insight to the behavior of the diffusion coefficient, we consider a class of systems for which $D(t \to \infty \mid \rho)$ is *independent* of ρ. First, as a concrete, but trivial, example, consider random walkers moving in free space, but in the presence of a uniform den-

sity of sinks. The number of walkers decays exponentially in time, but the surviving walkers move the same distance that they would have without the sinks; thus, $D(t \mid \rho) = D(t \mid \rho = 0)$. When the distribution of sinks is not uniform, $D(t \mid \rho)$ no longer equals $D(t \mid \rho = 0)$.

Consider next a pore space comprised of straight capillary tubes as in Fig. 1(a). The presence of interface relaxation obviously has an important effect on the magnetization, $M(\mathbf{k} = 0, t)$, but has no effect on the long-time diffusion coefficient. Formally, separation of coordinates implies that the Green's function (6a) factorizes into a product of a function of the distance along the tube axis and a function of the transverse distance. The latter function does, indeed, depend on ρ. However, in the long-time limit, only the *axial* contribution to the mean square displacement counts, and this is controlled by the (ρ independent) axial Green's function. If we picture the diffusion in discrete terms (i.e., in terms of random walk paths) the same conclusion follows once we note that steps in the axial and transverse directions are independent and that the mean square displacement at long times is controlled by the axial steps. Essentially the same lines of argument can be applied to a model in which the pore space is viewed as a collection of slowly winding and twisting capillary tubes, each with constant cross section [Fig. 1(b)].

In Fig. 2 we show a model in which the pore space consists of straight tubes connected to an array of "dead end" channels. If $\rho = 0$, the presence of the dead ends will certainly decrease the limiting value of the diffusion coefficient below the value corresponding to just straight tubes. Physically, those walkers that stray into the dead ends tend to make much less progress in the axial direction. Now, suppose we turn on interface relaxation. Molecules that enter the dead end regions are very efficiently eliminated (demagnetized) and do not, therefore, contribute to the mean square axial displacement. Thus the effective diffusion coefficient is *increased* by the presence of wall relaxation and, as $\rho \to \infty$, $D(t \mid \rho)$ approaches a value characteristic of the original straight tube.

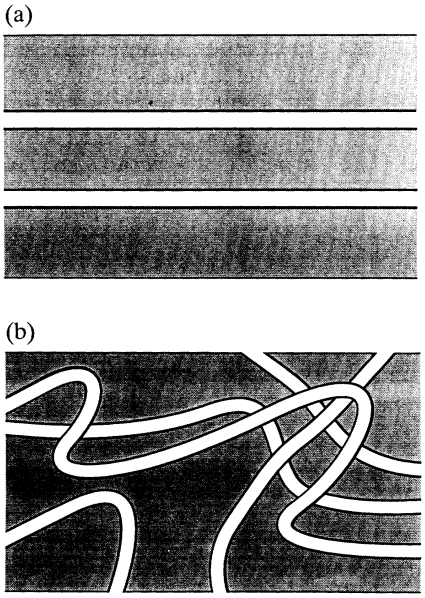

FIG. 1. (a) A pore space made of straight tubes. (b) A pore space comprised of a number of winding but nonintersecting tubes.

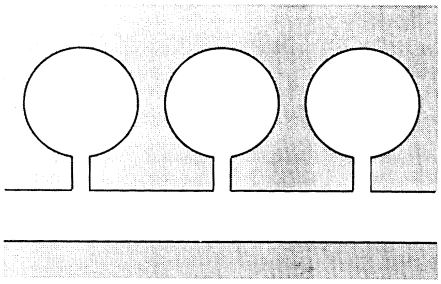

FIG. 2. A pore space made of straight tubes connected to "dead ends" by narrow throats.

While the above example illustrates that, in principle, ρ can act to increase the diffusion coefficient, in most systems of interest the opposite trend is to be expected. A model geometry that is sometimes used to study a class of porous media is shown in Fig. 3. Here we have a system comprised of relatively large pores connected by narrow throats. If $\rho = 0$, the throats control the final value of D_{eff} because they provide roughly one dimensional links between the larger pores where the diffusion can be quite close to the value characteristic of the bulk fluid. However, once $\rho \neq 0$, relaxation proceeds very efficiently as molecules move down the throats, and the probability for diffusing large distances is greatly diminished. Thus we expect a decrease in the limiting value of $D(t \mid \rho)$ whose magnitude is proportional to ρ (at least as $\rho \to 0$) and is controlled by the throat *length*. Physically, the walkers most likely to survive in this geometry are those that remain confined within a *single* pore. On the other hand, if the throat lengths are decreased to the point where the pore geometry is as shown in Fig. 4, then we expect surface relaxation to have relatively little effect on the limiting behavior of the diffusion coefficient. Here the throats are reduced to simple apertures whose width limits the $\rho = 0$ diffusion coefficient but which do not provide especially efficient regions for relaxation when $\rho \neq 0$.

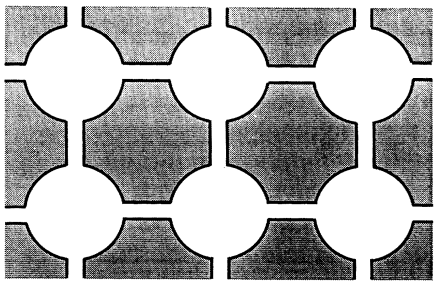

FIG. 3. A pore space comprised of large pores connected by narrow throats.

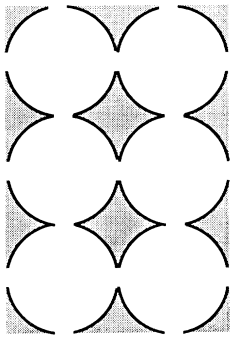

FIG. 4. A pore space in which the length of the connecting throats (shown in Fig. 3) has been decreased to zero while keeping the throat width constant.

How are these qualitative arguments reconciled with Eq. (8)? For simplicity, we take the view that the pore geometry acts to divide the random walkers into two populations: N_{long} walkers that diffuse a long distance, $\langle r^2(t)\rangle_{\text{long}}$, and N_{short} walkers that diffuse a short distance, $\langle r^2(t)\rangle_{\text{short}}$. Roughly, Eq. (8) then reduces to

$$\langle r^2(t)\rangle_s = \frac{N_{\text{long}}\langle r^2(t)\rangle_{\text{long}} + N_{\text{short}}\langle r^2(t)\rangle_{\text{short}}}{N_{\text{long}} + N_{\text{short}}} . \tag{10}$$

If $\rho = 0$, N_{long} and N_{short} do not vary with time. Suppose that, for $\rho \neq 0$, we find at long times that $N_{\text{long}} \gg N_{\text{short}}$ so that $\langle r^2(t)\rangle_s \approx \langle r^2(t)\rangle_{\text{long}}$. It follows that $D(t \mid \rho) \geq D(t \mid \rho = 0)$ as in the "dead end" model above where on physical grounds we expect $N_{\text{long}} \gg N_{\text{short}}$. On the other hand, in the "pore and throat" model we expect $N_{\text{long}} \ll N_{\text{short}}$ (for $\rho \neq 0$) so that $\langle r^2(t)\rangle_s \approx \langle r^2(t)\rangle_{\text{short}}$ and $D(t \mid \rho) \leq D(t \mid \rho = 0)$. In the case of dilute suspensions of spherical grains this kind of separation is not easily made; nevertheless, the analytic results presented in Sec. III A show that $D(t \mid \rho) \leq D(t \mid \rho = 0)$.

C. Short-time expansion

To derive a formal perturbative expansion we follow an approach that is similar to the one developed in our previous paper on the short-time behavior of $D(t \mid \rho)$.[9] We work with the Laplace representation of Eqs. (6a) and (7):

$$s\tilde{G}(\mathbf{r},\mathbf{r}',s) - \delta(\mathbf{r}-\mathbf{r}') = D_0\nabla^2\tilde{G}(\mathbf{r},\mathbf{r}',s) \tag{11a}$$

and

$$D_0\hat{\mathbf{n}}\cdot\nabla\tilde{G}(\mathbf{r},\mathbf{r}',s) + \rho\tilde{G}(\mathbf{r},\mathbf{r}',s)\mid_{\mathbf{r}\in\Sigma} = 0 . \tag{11b}$$

Now, let $\tilde{G}_0(\mathbf{r}',\mathbf{r}'',s)$ be the $\rho = 0$ Green's function defined by the equations

$$s\tilde{G}_0(\mathbf{r}',\mathbf{r}'',s) - \delta(\mathbf{r}'-\mathbf{r}'') = D_0\nabla^2\tilde{G}_0(\mathbf{r}',\mathbf{r}'',s) \tag{12a}$$

and

$$\hat{\mathbf{n}}\cdot\nabla\tilde{G}_0(\mathbf{r}',\mathbf{r}'',s)\mid_{\mathbf{r}\in\Sigma} = 0 . \tag{12b}$$

Multiplying Eq. (11a) by $\tilde{G}_0(\mathbf{r}',\mathbf{r}'',s)$, Eq. (12a) by $\tilde{G}(\mathbf{r},\mathbf{r}',s)$, integrating over $\mathbf{r}'$, and subtracting we have

$$\tilde{G}(\mathbf{r},\mathbf{r}'',s) = \tilde{G}_0(\mathbf{r},\mathbf{r}'',s) - \rho\int d\sigma'\tilde{G}(\mathbf{r},\mathbf{r}',s)\tilde{G}_0(\mathbf{r}',\mathbf{r}'',s) \tag{13a}$$

or, in the time domain,

$$G(\mathbf{r},\mathbf{r}'',t) = G_0(\mathbf{r},\mathbf{r}'',t) - \rho\int d\sigma'\int_0^t dt' G(\mathbf{r},\mathbf{r}',t')G_0(\mathbf{r}',\mathbf{r}'',t-t') . \tag{13b}$$

Here we have made use of the boundary condition (11b) and employed Stokes' theorem to convert a volume integral to a surface integral.

While the preceding equations are correct, their utility in connection with the long-time behavior of the diffusion problem is rather limited. The Green's function $G(\mathbf{r},\mathbf{r}',t)$ decays exponentially because of enhanced relaxation at the interface. By contrast, $G_0(\mathbf{r},\mathbf{r}',t)$ does not decay and therefore, as $t\to\infty$, provides a very poor starting point for a perturbation series. Nevertheless, if ρ is sufficiently small, perturbation series derived from (13) can still be quite useful. For example, in a periodic system, suppose that t is large enough that the diffusion length, $[D(t \mid 0)t]^{1/2}$, is several times larger than the unit cell length. At such times the diffusion coefficient will have nearly reached its asymptotic limit. If the value of ρ is small enough that the magnetization has not decayed appreciably, a perturbation expansion generated from the above equations should be valid.

To illustrate the use of Eq. (13b) let us first consider the influence of ρ on the decay of the magnetization $M(t) = M(\mathbf{k}=0,t)$. Keeping terms up to linear in ρ, we have

$$M(t) = \frac{1}{V_p}\int d\mathbf{r}d\mathbf{r}''G(\mathbf{r},\mathbf{r}'',t)$$

$$= \frac{1}{V_p}\int d\mathbf{r}d\mathbf{r}''G_0(\mathbf{r},\mathbf{r}'',t) - \frac{\rho}{V_p}\int d\mathbf{r}d\sigma'd\mathbf{r}''\int_0^t dt' G_0(\mathbf{r},\mathbf{r}',t')G_0(\mathbf{r}',\mathbf{r}'',t-t') + \cdots . \tag{14}$$

If $\rho = 0$, there is no decay and $V_p^{-1} \int d\mathbf{r}d\mathbf{r}'' G_0(\mathbf{r},\mathbf{r}'',t) = 1$. The second term in (14) may then conveniently be written in terms of an effective time-dependent surface area, $\mathcal{S}(t)$,

$$M(t) = 1 - \frac{\rho \mathcal{S}(t) t}{V_p} + \cdots \approx \exp\left[-\frac{\rho \mathcal{S}(t) t}{V_p}\right] , \tag{15a}$$

where

$$\mathcal{S}(t) \equiv \frac{1}{t} \int d\mathbf{r}d\sigma' d\mathbf{r}'' \int_0^t dt' G_0(\mathbf{r},\mathbf{r}',t') G_0(\mathbf{r}',\mathbf{r}'',t-t') . \tag{15b}$$

Note that as $t \to 0, G_0(\mathbf{r},\mathbf{r}'',t) \to \delta(\mathbf{r}-\mathbf{r}'')$, and so $\mathcal{S}(t) \to S$, where S is the pore surface area. Thus, as expected, (15a) properly describes the short-time limit

$$\lim_{t\to 0}\left[\frac{dM(t)}{dt}\right] = \frac{\rho S}{V_p} . \tag{16}$$

In addition, it is easily shown that $\mathcal{S}(t) = S$ for all t if the pore space can be described in terms of a discrete normal mode spectrum.[18] Returning to Eq. (13b), we consider next the analog of Eq. (14) for the diffusion coefficient. Recalling Eq. (8), the leading effects of surface relaxation may be written as

$$D(t \mid \rho) = D(t \mid 0)\left[1 - \frac{\rho}{D(t \mid 0)} \{L_1(t) - L_2(t)\}\right] , \tag{17}$$

where

$$D(t \mid 0) = \frac{1}{6tV_p} \int (\mathbf{r}-\mathbf{r}'')^2 G_0(\mathbf{r},\mathbf{r}'',t) d\mathbf{r}d\mathbf{r}'' \tag{18}$$

and

$$L_1(t) = \frac{1}{6tV_p} \int_0^t dt' \int (\mathbf{r}-\mathbf{r}'')^2 G_0(\mathbf{r},\mathbf{r}',t-t') G_0(\mathbf{r}',\mathbf{r}'',t') d\mathbf{r}d\sigma' d\mathbf{r}'' , \tag{19a}$$

$$L_2(t) = \frac{D(t \mid 0)}{V_p} \int_0^t dt' \int G_0(\mathbf{r},\mathbf{r}',t-t') G_0(\mathbf{r}',\mathbf{r}'',t') d\mathbf{r}d\sigma' d\mathbf{r}'' = \frac{D(t \mid 0)\mathcal{S}(t) t}{V_p} . \tag{19b}$$

We emphasize that Eq. (17) represents a short-time expansion of $D(t \mid \rho)$. As described above, its utility is limited to the case of very small ρ values. It is interesting to note that the two length parameters, $L_1(t)$ and $L_2(t)$, enter Eq. (17) with opposite signs. This is to be expected based on our earlier discussion of the influence of ρ on Eq. (8).

III. CALCULATIONS ON PERIODIC SYSTEMS

A. Nonoverlapping spherical grains

In this section we consider the effective diffusion coefficient for a periodic array of solid spheres, each of radius a, immersed in the fluid. The PFGSE amplitude, $m(\mathbf{r},t)$, obeys Eqs. (6a) and (7) and is most conveniently written in terms of the eigenfunctions, $m(\mathbf{r},t) = m(\mathbf{r})e^{-Et}$, where

$$(\nabla^2 + q^2) m(\mathbf{r}) = 0 , \tag{20}$$

$q^2 \equiv E/D_0$, and E is the eigenvalue. The structure of this eigenvalue problem is quite similar to that of many problems encountered in the electronic theory of solids. Indeed, we will see that the variable q^2 in Eq. (20) corresponds to the electron energy and that boundary condition

$$[D_0 \hat{\mathbf{n}} \cdot \nabla m(\mathbf{r}) + \rho m(\mathbf{r})]_{r=a} = 0 \tag{21}$$

gives rise to the analog of the scattering phase shifts, $\{\delta_l(q)\}$. Within this framework, $D_{\text{eff}}(\rho)$ is related to the curvature at the bottom of the lowest energy band and is analogous to the effective mass.

Let us begin by expressing $M(\mathbf{k},t)$ in terms of eigenfunctions[7]

$$m_{n\mathbf{p}}(\mathbf{r}) = e^{i\mathbf{p}\cdot\mathbf{r}} u_{n\mathbf{p}}(\mathbf{r}) , \tag{22}$$

which satisfy the Bloch-Floquet theorem. Here n is a band index, the function $u_{n\mathbf{p}}(\mathbf{r})$ has the translational periodicity of the underlying Bravais lattice, and $\mathbf{p}$ is a vector in the first Brillouin zone (BZ) of the reciprocal lattice. Given an arbitrary momentum vector $\mathbf{k}$, the magnetization density can be written as

$$M(\mathbf{k},t) = \sum_n e^{-E_n(\mathbf{p})t} \mid \tilde{u}_{n,\mathbf{p}}(\mathbf{K}) \mid^2 . \tag{23}$$

Here $\mathbf{K}$ is the unique reciprocal lattice vector that returns $\mathbf{k}$ to the first zone, i.e., $\mathbf{k} = \mathbf{p} + \mathbf{K}$ and

$$\tilde{u}_{n,\mathbf{p}}(\mathbf{K}) \equiv \frac{1}{\phi\Omega} \int \exp(i\mathbf{K}\cdot\mathbf{r}) u_{n,\mathbf{p}}(\mathbf{r}) d\mathbf{r} , \tag{24}$$

with the integration confined to a single unit cell of volume Ω. The splitting between the two lowest "energy" bands will be of order of D_0/b^2, where b is the lattice constant. For $t \gg b^2/D_0$, the lowest band controls the sum in Eq. (23). Assuming that the effective mass tensor is isotropic (as it will be in cubic systems) $E_0(\mathbf{p}) \approx p^2 D_{\text{eff}}$, and we have (for $p \ll b^{-1}$)

$$M(\mathbf{k},t) = e^{-p^2 D_{\text{eff}} t} \mid \tilde{u}_{0,\mathbf{p}}(\mathbf{K}) \mid^2 . \tag{25}$$

Returning to Eqs. (20) and (21) we proceed to evaluate D_{eff} by estimating the curvature of the lowest energy band at the center of BZ for a periodic array of solid spheres immersed in a fluid. It is convenient here to use the formalism of scattering theory. Following Schwartz

and Johnson[19] the eigenvalues are obtained by solving the secular equation

$$|| \tau_l^{-1}(q)\delta_{LL'} - B_{LL'}(\mathbf{p}|q) ||= 0 \ . \tag{26}$$

Here $L = (l, m)$ is a composite angular momentum index where $l(m)$ is the orbital (azimuthal) quantum number. The quantities $B_{LL'}(\mathbf{p}|q)$ are known as structure functions and depend only on the geometry of the lattice. The energy-shell scattering matrix τ_l for the lth partial wave can be expressed in terms of the phase shifts $\delta_l(q)$:

$$\tau_l(q) = -\frac{1}{q} e^{i\delta_l(q)} \sin[\delta_l(q)]. \tag{27}$$

The phase shifts are calculated by applying the boundary condition (21) at the surface of each sphere of radius a,

$$\tan\delta_l(q) = \frac{j_l'(qa) - (\rho a/D_0) j_l(qa)}{n_l'(qa) - (\rho a/D_0) n_l(qa)} \ , \tag{28}$$

where $j_l(x)$ and $n_l(x)$ denote, respectively, spherical Bessel and Neumann functions, and the prime indicates a derivative with respect to x. It can be seen from (28) that $\rho a/D_0$ is the parameter which controls the phase shifts. We find that for many cases of interest, $\tilde{\rho} = \rho a/D_0$ is a small parameter.[17]

For simplicity, we choose a simple cubic system where the eigenvalues are independent of $\hat{\mathbf{p}}$, as $| \mathbf{p} |\to 0$. The eigenvalues $E(\mathbf{p}) \equiv D_0 q^2(\mathbf{p})$ depend on the number of angular momentum considered. Taking $l_{\max} = 1$, we find from Eq. (14) of Ref. 19 that the eigenvalues are given by

$$[B_{00}' + q\cot\delta_0(q)]\,[B_{11}' + q\cot\delta_1(q)] - B_{01}' B_{10}' = 0 \ , \tag{29}$$

where $B'_{LL'}(\mathbf{p}|q) = B_{LL'}(\mathbf{p}|q) + iq\delta_{LL'}$,

$$B_{00}' = \frac{4\pi n}{q^2 - p^2}, \quad B_{11}' = \frac{4\pi n}{q^2 - p^2}\left[1 + 2\frac{p^2}{q^2}\right] \ , \tag{30}$$

and

$$B_{01}' = B_{10}' = \frac{4\pi n\sqrt{3}}{q^2 - p^2}\frac{p}{q} \ . \tag{31}$$

Here n is the density of spheres per unit volume. The volume fraction of solid $f = 1 - \phi$ and porosity ϕ are related to the sphere size a and density n via $f = 1 - \phi = 4\pi n a^3/3$. Equation (29) simplifies to

$$q^2 = \gamma_0 + p^2\frac{1 - 2\alpha}{1 + \alpha} \ , \tag{32}$$

where

$$\gamma_0 = \frac{4\pi n}{q}\tan\delta_0(q), \quad \alpha = \frac{4\pi n}{q^3}\tan\delta_1(q) \tag{33}$$

are independent of p. In the limit $\rho a/D_0 << 1$ the roots are obtained by expanding the Bessel and Neumann functions for small arguments $qa << 1$. We find that the bottom of the lowest energy band moves from $q = 0$ (when $\rho = 0$) to q_0 where

$$(q_0 a)^2 = 3f\frac{\tilde{\rho}}{1 - f + (1 + 2f)\tilde{\rho}} \approx \frac{3f}{1 - f}\tilde{\rho}. \tag{34}$$

This implies that the long-time decay rate is a simple exponential:

$$M(k = 0, t) = e^{-D_0 q_0^2 t} = e^{-\rho S t/V_p} \ , \tag{35}$$

where $S/V_p = 3f/(1 - f)a$ in this simple case. We noted in connection with Eq. (16) that this is exactly the decay rate of the overall magnetization at the earliest times. That the late-time decay constant is approximately equal to the early-time decay rate is a reflection of the fact that we chose a simple geometry and assumed that $\tilde{\rho} << 1$. In this case, the diffusion time across unit cell is small compared to the decay time. (Recall, that this was the condition given for the validity of the results in Sec. II C.) In the literature, this condition is known as the fast diffusion limit.[20] Equation (32) gives the curvature at the bottom of the band:

$$D_{\text{eff}}(\rho) = \frac{D_0}{1 - f} \times \frac{2 + \tilde{\rho} - 2f[1 - \tilde{\rho} - q_0^2 a^2(3 - \tilde{\rho})/10]}{2 + \tilde{\rho} + f[1 - \tilde{\rho} - q_0^2 a^2(3 - \tilde{\rho})/10]} \ . \tag{36}$$

The influence of ρ is to reduce $D_{\text{eff}}(\rho)$ from its electrical equivalent. Expanding the above equation in $\tilde{\rho}$,

$$\frac{D_{\text{eff}}(\rho)}{D_0} = \frac{2}{3 - \phi} - \frac{3}{5} f\tilde{\rho}\frac{5 + 20f + 2f^2}{(1 - f)^2(2 + f)^2} + O(\tilde{\rho}^2), \tag{37}$$

brings out the interplay of $\tilde{\rho}$ with geometry. Indeed, Eq. (37) is of the same form as the perturbative expansions derived in Sec. II C. As expected, this $D_{\text{eff}}(\rho)$ is identical to that obtained from the electrical conductivity when $\rho = 0$, since for a dilute array of spheres, $1/F = 2\phi/(3 - \phi)$.[21] Note that the further decrease in the diffusion coefficient is proportional to $\tilde{\rho} f/(1 - f)^2$. Thus the present results suggest that $D_{\text{eff}}(\rho)$ will decrease as the porosity decreases. Of course, as the sphere radius increases, the approximation $q_0 a \ll 1$ breaks down, we can no longer take $l_{\max} = 1$, and the analysis of the secular determinant (26) becomes more complicated. Nevertheless, $D_{\text{eff}}(\rho)$ may reasonably be expected to decrease rapidly as the porosity decreases.

B. Perturbation theory

While the results derived in the preceding subsection give an explicit formula for the long-time diffusion coefficient in the limit of small ρ, the methods of scattering theory are suitable only for a special category of periodic structures, viz., nonoverlapping spherical grains. By contrast, in most porous media of interest the grains are nonspherical and well consolidated. Since we are interested in long wavelength behavior of the lowest "energy band," it is natural to employ a version of perturbation theory to study the effects of ρ on the effective diffusion coefficient.[22] Beginning with the eigenfunctions (22) and recalling the derivation of (13a), we have the identity

$$\left[E_n(\mathbf{p}) - E_m^{(0)}(\mathbf{p})\right] \int d\mathbf{r}\, u_{n\mathbf{p}}^*(\mathbf{r}) u_{m\mathbf{p}}^{(0)}(\mathbf{r}) = \rho \int dS\, u_{n\mathbf{p}}^*(\mathbf{r}_s) u_{m\mathbf{p}}^{(0)}(\mathbf{r}_s) \ , \tag{38}$$

where the superscript (0) denotes quantities associated with the limit $\rho = 0$. Since the functions $\{u^{(0)}_{n\mathbf{p}}(\mathbf{r})\}$ form a complete set for each wave vector $\mathbf{p}$ in the Brillouin zone, we can develop a perturbation series based on the expansion

$$u_{1\mathbf{p}}(\mathbf{r}) = \sum_n C_n u^{(0)}_{n\mathbf{p}}(\mathbf{r}) \ . \tag{39}$$

The lowest band of eigenvalues, $E_1(\mathbf{p})$, through second order in ρ is given by

$$E_1(\mathbf{p}) = E^{(0)}_1(\mathbf{p}) + \rho M_{11}(\mathbf{p}) \tag{40}$$

$$+ \sum_{n\neq 1} \frac{\rho^2 \mid M_{1n}(\mathbf{p}) \mid^2}{E^{(0)}_1(\mathbf{p}) - E^{(0)}_n(\mathbf{p})} \ , \tag{41}$$

where

$$M_{nm}(\mathbf{p}) \equiv \int dS \, \{u^{(0)}_{n\mathbf{p}}(\mathbf{r}_s)\}^* u^{(0)}_{m\mathbf{p}}(\mathbf{r}_s) \ . \tag{42}$$

To first order in ρ the effective diffusion coefficient is

$$D_{\text{eff}}(\rho) = D_{\text{eff}}(0)\left[1 - \frac{\rho}{D_{\text{eff}}(0)}\frac{dM_{11}}{dp^2}\right] \equiv D_{\text{eff}}(0)\left[1 - \frac{\rho L}{D_{\text{eff}}(0)}\right] \ . \tag{43}$$

This equation relates the length scale, L, that controls the ρ dependence of $D_{\text{eff}}(\rho)$ to the $\mathbf{p}$ dependence of the $\rho = 0$ eigenfunctions through the matrix element $M_{11}(\mathbf{p})$. One way of calculating this $\mathbf{p}$ dependence is to use a perturbation series based on the $\mathbf{p} = 0$ solutions. Recalling Eqs. (20), (21), and (22), we have

$$-E^{(0)}_n(\mathbf{p})u^{(0)}_{n\mathbf{p}} = D_0\nabla^2 u^{(0)}_{n\mathbf{p}} + D_0\left[2i\mathbf{p}\cdot\nabla - p^2\right]u^{(0)}_{n\mathbf{p}} \equiv D_0\left[\nabla^2 + V(\mathbf{p})\right]u^{(0)}_{n\mathbf{p}} \tag{44}$$

and

$$[D_0\hat{\mathbf{n}}\cdot\nabla u^{(0)}_{n\mathbf{p}} + \mathbf{p}\cdot\hat{\mathbf{n}}u^{(0)}_{n\mathbf{p}}]_{\mathbf{r}\in\Sigma} = 0 \ . \tag{45}$$

Assuming that the solutions at $\mathbf{p} = 0$ are known, we seek an expansion of the form

$$u^{(0)}_{1\mathbf{p}}(\mathbf{r}) = \sum_n c_n u^{(0)}_{n0}(\mathbf{r}) \ . \tag{46}$$

Straightforward algebra leads to the linear equation

$$\sum_n \left[\left\{E^{(0)}_1(\mathbf{p}) - E^{(0)}_1(\mathbf{0})\right\}\delta_{1n} + D_0 V_{1n}(\mathbf{p}) - D_0 i\mathbf{p}\cdot\mathbf{Q}_{1n}\right]c_n = 0 \ , \tag{47}$$

where, for systems with cubic symmetry, the matrix elements reduce to

$$\mathbf{Q}_{1n} \equiv (1-\delta_{1n})\int \{u^{(0)}_{10}(\mathbf{r}_s)\}^* u^{(0)}_{n0}(\mathbf{r}_s)\hat{\mathbf{n}}\, dS \tag{48}$$

and

$$V_{1n}(\mathbf{p}) \equiv \int \{u^{(0)}_{10}(\mathbf{r})\}^* V(\mathbf{p}) u^{(0)}_{n0}(\mathbf{r})\, d\mathbf{r} = -p^2\delta_{1n} + 2i\mathbf{p}\cdot\int \{u^{(0)}_{10}(\mathbf{r})\}^*\nabla u^{(0)}_{n0}(\mathbf{r})\, d\mathbf{r}$$
$$= -p^2\delta_{1n} + 2i(1-\delta_{1n})\mathbf{p}\cdot\mathbf{Q}_{1n} \ . \tag{49}$$

Note that the last of these equations indicates that the off diagonal coupling in Eq. (47) simplfies to $D_0 V_{1n}(\mathbf{p}) - D_0 i\mathbf{p}\cdot\mathbf{Q}_{1n} = D_0 i\mathbf{p}\cdot\mathbf{Q}_{1n}$. The momentum dependence of the eigenstates is then given by a series of the form

$$u^{(0)}_{1\mathbf{p}}(\mathbf{r}) = u^{(0)}_{10}(\mathbf{r}) + \sum_{n\neq 1}\frac{D_0 i\mathbf{p}\cdot\mathbf{Q}_{1n}u^{(0)}_{n0}(\mathbf{r})}{E^{(0)}_n(\mathbf{0}) - D_0 p^2} + \cdots \ . \tag{50}$$

Substituting this expansion into Eq. (43), we can calculate directly the momentum derivatives of $M_{11}(\mathbf{p})$. For example, from the term dispalyed in (50), we have

$$\lim_{p\to 0}\frac{dM}{dp^2} = \sum_{n,m\neq 1}\sum_\alpha \frac{D_0^2 M_{nm}(\mathbf{0})}{E^{(0)}_n(\mathbf{0})E^{(0)}_m(\mathbf{0})}\{\mathbf{Q}_{1n}\}^*_\alpha\{\mathbf{Q}_{1m}\}_\alpha + \cdots \ . \tag{51}$$

Additional contributions to $D_{\text{eff}}(\rho)$ are obtained from the terms in the series (50) of second order in $\mathbf{p}$.

IV. NUMERICAL SIMULATIONS

Calculations of the kind described in the preceding section are valuable in that they provide an unambiguous analytic framework within which the behavior of $D_{\text{eff}}(\rho)$ can be estimated. In more complex geometries, however, the utility of these techniques is quite limited, and numerical simulations of diffusion are the only computational technique available. Indeed, even within the context of ordered, nonoverlapping, sphere packs, the analysis of $D(t \mid \rho)$ becomes rather involved as the sphere radius increases. [Many angular momenta are required for convergence of the secular Eq. (26) and detailed numerical calculations are required.] By contrast, simulations techniques are applicable in both ordered and disordered geometries and can even be carried over to the consoli-

dation regime in which the spherical grains overlap.

In Figs. 5–7 we present the results of random walk simulations on a number of ordered cubic packings and on one disordered monosized sphere pack.[24] In these simulations, a random walker moves through the pore space taking steps of fixed length, ϵ. In ordered systems the value of ϵ is typically chosen in the range $0.005 \leq \epsilon/b \leq 0.01$ where b is the length of the unit cell edge. Here the calculation is carried out in a single unit cell with periodic boundary conditions used to keep track of diffusion into neighboring cells. For the disordered sphere pack the step size was taken equal to $0.01b$ where b is the grain diameter. Here we employed a single large representation of the packing [(20 grains) × (20 grains) × (40 grains) in the x, y, and z directions, respectively] with periodic boundary conditions in the x and y directions. This representation is large enough to provide an effective average over different spatial configurations of the grains so that there is no need for configuration averaging. In both the ordered and disordered cases, walkers were released from initial positions chosen randomly throughout the pore space in order to properly reflect the experimental situation. (For the

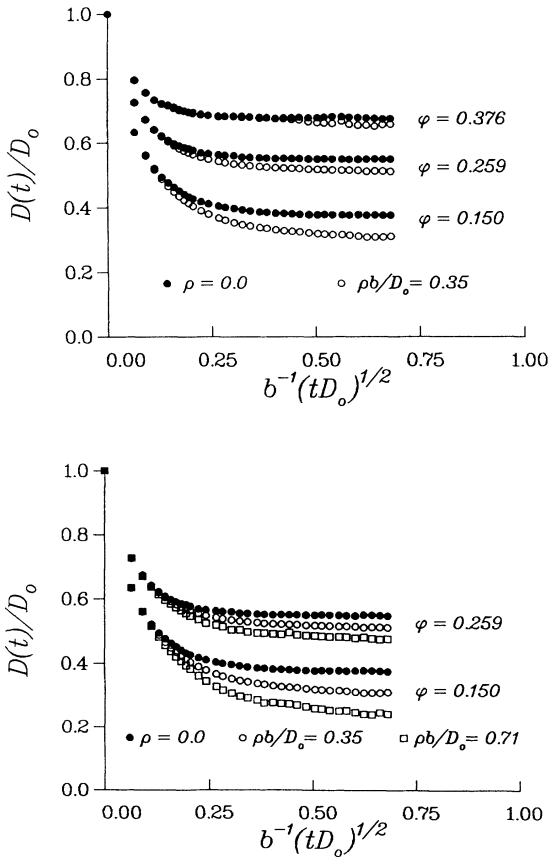

FIG. 5. Simulation results for fcc packings. Upper panel: three porosities are compared in calculations with $\gamma = 0$ and $\gamma = 0.0025$. Lower panel: for the two lower porosities, calculations with $\gamma = 0$, $\gamma = 0.0025$, and $\gamma = 0.0050$ are compared. Here, as in Figs. 6 and 7, the quantities plotted on both axes are dimensionless.

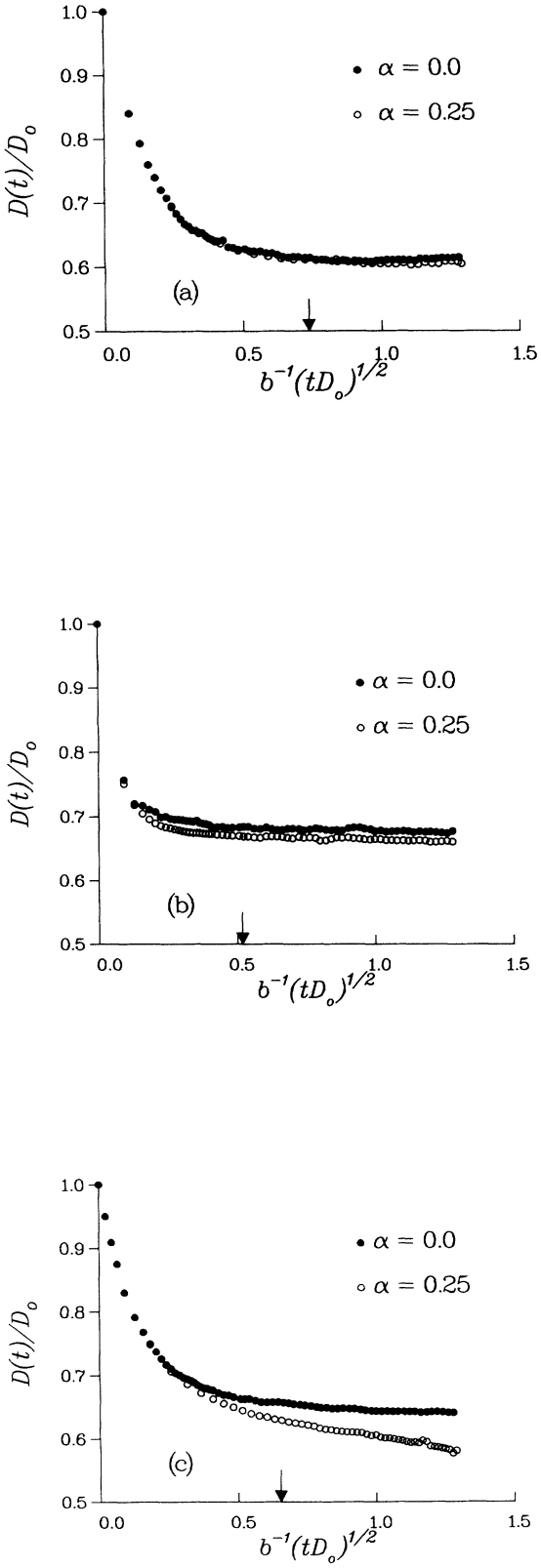

FIG. 6. Simulation results for ordered and disordered packings are compared. Here $\gamma = 0.0025$ and the cube edge, $b = 2.0$, for the ordered packings in (a) and (b). In (c) the grain diameter, $b = 2.0$. In all three figures the arrow on the horizontal axis marks the $t = T_1 = V_p/(\rho S)$ position, and $\phi = 0.376$.

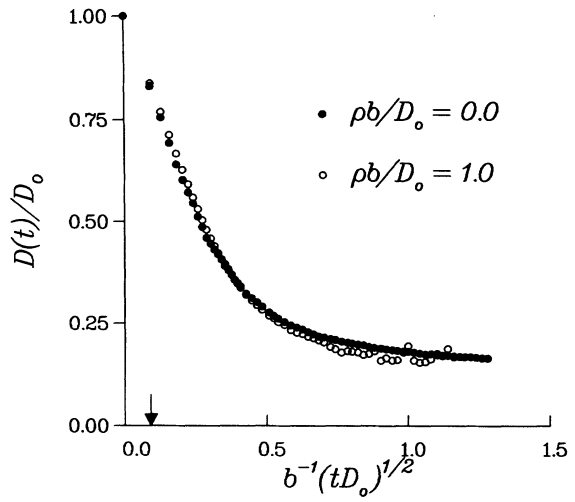

FIG. 7. Simulation results for a cubic swiss cheese model in which the pore throat diameter is 0.10 in units where the cube edge, $b = 2.0$. Calculations with $\gamma = 0.0$ and $\gamma = 0.05$ are compared. The arrow marks the $t = T_1 = V_p/(\rho S)$ position.

disordered packing, the z position of the starting point was taken within a band of values chosen such that the walker never sampled the regions at the very top or bottom of the packing.) The implementation of the boundary condition (7) is identical in ordered and disordered systems. In the case $\rho = 0$, we have *blind* reflection at the pore grain interface.[24] For $\rho \neq 0$, when a walker encounters the interface the proton magnetization decays (i.e., the walker is "killed") with probability γ (per unit time step, τ). In the case of weakly enhanced interfacial decay the relation between γ and the phenomenological parameter ρ is[23],[24]

$$\rho = \frac{D_0\gamma}{\epsilon} = \frac{\epsilon\gamma}{6\tau}, \tag{52}$$

where, in the second equality, we have used the identity $D_0 = \epsilon^2/(6\tau)$. Given specific values for the unit cell edge or the grain diameter and D_0, we can easily convert the results of computer simulations into physical units.

In Fig. 5(a) we compare the results of simulations on three ordered fcc packings of spherical grains. Here the lattice constant, b, is fixed and the porosity is varied by changing the grain radius. [The $\phi = 0.376$ system corresponds to isolated spheres, $\phi = 0.259$ corresponds to close packed (touching) spheres, and $\phi = 0.150$ corresponds to overlapping spheres.] At each porosity we compare calculations in which $\rho = 0$ and $\rho b/D_0 = 0.35$.[25] Recalling Eq. (37), we expect the effect of finite surface relaxation on $D(t \mid \rho)$ to become more pronounced as the porosity decreases. This trend is quite evident in Fig. 5(a). In Fig. 5(b) we verify that the shift in $D_{\text{eff}}(\rho)$ is indeed linear in ρ. For the two porosities considered in Fig. 5(b), the numerical data can be used to estimate the length L entering Eq. (43) and we find $L = 0.10b$ ($\phi = 0.259$) and $L = 0.19b$ ($\phi = 0.150$). The fact that L increases as ϕ decreases is in qualitative accord with Eq. (37). Physically, this result indicates that surface relaxation is effectively limiting diffusion through the narrowest channels of the pore space in this simple geometry.

It should be noted that the number of walkers required to achieve statistically significant results varies widely for the cases considered in Fig. 5. For $\rho b/D_0 = 0$ (i.e., $\gamma = 0$) a few thousand walkers are sufficient. When $\rho b/D_0 = 0.35$ several hundred thousand walkers are required and the number of walkers must be increased as the porosity is reduced because diffusion from pore to pore is being made more difficult. For $\rho b/D_0 = 0.71$ several 10^6 walkers are needed to obtain accurate results with the number again increasing as ϕ decreses. Of course, computational time does not increase directly with the number of walkers because, with nonvanishing ρ, most of the walkers are killed after a relatively small number of time steps. Indeed, a large number of walkers is required just so that at long times enough survive to give a significant sample.

In Fig. 6 we compare calculations on three different packings, sc, fcc, and dense random, all of which have the same porosity, $\phi = 0.376$. In each case $\rho = 0$ results are compared with results for small ρ. Note, first, that the asymptotic values for the three $\rho = 0$ calculations are not identical, as different formation factors are to be expected for different geometries. The differences here are small and all the values are close to the rule of thumb value for sphere packs, $D_{\text{eff}}/D_0 \approx \phi^{1/2}$.[21] The calculations shown in Figs. 6(a) and 6(b) both indicate a very small shift of $D(t \mid \rho)$ to lower values at long times for $\rho \neq 0$. A larger effect is seen in Fig. 6(c) where results for a dense random sphere pack are presented. This increase is not necessarily associated with the randomness of the packing directly. As we have seen above, in periodic models, such as the pore-throat model, a similar reduction was due to a decrease in the throat aspect ratio (diameter/length). In open sphere pack geometries, of the kind considered in Sec. III A, this separation into pores and throats is not possible. We note that in the random packing, the narrow throats connecting pores are smaller than the corresponding regions in either of the two ordered packings (Fig. 8). In the unconsolidated fcc packing the "throats" are formed by *three* nonoverlapping coplanar spheres, and are much larger than the throats typically found in dense random packings. In the simple cubic case, the throats are formed by *four* spheres and are again larger than those found in the random packing. Note that in Fig. 6(c) the results for $\rho \neq 0$ have not yet reached their long-time limit. Physically, because the throats are longer and narrower in this case, it takes more time for a random walker to average its motion over many pores and throats than in either the simple or face centered cubic packing.

In Fig. 7 calculations with a small surface relaxation value are again compared with the results of $\rho = 0$ simulations.[26] Here the system is a three-dimensional simple cubic version of the swiss cheese geometry pictured in Fig. 4. The pores are essentially spherical, their radius, however, is taken large enough so that they overlap to form zero-length apertures whose diameter equals 0.05 times the cube edge. Here we see that, as expected, the influence of ρ on the long-time behavior of the diffusion coefficient is greatly reduced. Even for observation

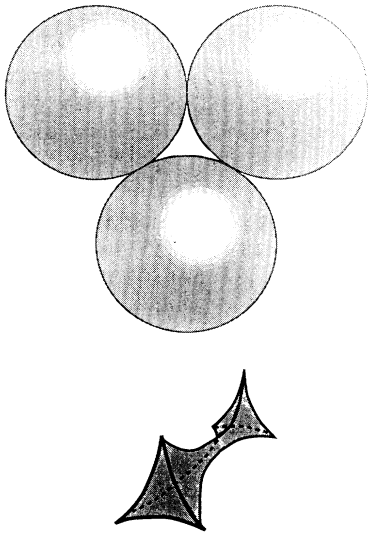

FIG. 8. Schematic representation of the throat formed by three touching spheres in a close packing environment. Throats of this kind are formed in a random packing with $\phi \approx 0.38$ and in a fcc packing with $\phi = 0.259$. The throats in a $\phi \approx 0.38$ fcc packing are formed by a similar configuration of *nonoverlapping* spheres.

times significantly greater than the effective relaxation time (shown by the arrow) the two calculations are in good agreement. As we argued in Sec. II, nonvanishing ρ values, in this case, do not greatly affect our ability to estimate the value of D_{eff}.

V. SUMMARY AND CONCLUSIONS

Electrical conductivity and PFGSE experiments both probe the physics of diffusion in the pore space of composite media. These two measurements yield the same diffusion coefficient only when enhanced surface relaxation and internal field inhomogeneities play no role in the NMR experiment and when interfacial conductivity can be neglected in the electrical problem. In addition, we must assume that the sample is not heterogeneous beyond the diffusion length scale (which is determined by both the NMR lifetime and the pore-space tortuosity). In this paper we have examined several aspects of the way that surface relaxation affects the behavior of $D(t \mid \rho)$. Our principal results are the following.

(i) On physical grounds one can see that in pore geometries with many "dead ends" surface relaxation will tend to increase the effective diffusion coefficient. By contrast, when the pore space contains long narrow throats connecting larger pores, the diffusion coefficient will typically decrease with ρ.

(ii) When the pore geometry is defined by an ordered packing of nonoverlapping grains, the PFGSE problem can be formulated in terms of a secular equation similar to those employed to study electronic energy bands. In the high porosity limit, this equation can be solved analytically to give the dependence of $D_{\text{eff}}(\rho)$ on ρ.

(iii) A perturbative form $D_{\text{eff}}(\rho) = D_{\text{eff}}(0)[1 - \rho L/D_{\text{eff}}(0)] + O(\rho^2)$ is suggested for a general homogeneous disordered medium. Here L is a length parameter roughly analogous to the Λ parameter of electrical conductivity.[15] In general L can be either positive or negative, depending on the pore geometry.

(iv) In more general pore geometries numerical simulations can be used to clarify the influence of ρ on the time dependence of the diffusion coefficient. This influence is greatest in systems where the pores are connected by long narrow throats, the *aspect ratio* of the throat being especially important.

ACKNOWLEDGMENTS

We thank M. Hurlimann, D. L. Johnson, and R. L. Kleinberg for useful discussions. Work at Harvard was supported in part by the National Science Foundation through the Harvard Materials Research Laboratory and Grant No. DMR91-15491.

[1] J. E. Tanner and E. O. Stejskal, J. Chem. Phys. **49**, 1768 (1968).
[2] P. T. Callaghan, Aust. J. Phys. **37**, 359 (1984).
[3] H. J. Vinegar and W. P Rothwell, U.S. Patent No. 471942 (1988).
[4] R. M. Cotts, Nature **351**, 467 (1991).
[5] P. T. Callaghan, D. MacGowan, K. J. Packer, and F. O. Zelaya, Nature **351**, 467 (1991); J. Magn. Res. **90**, 177 (1990).
[6] P. P. Mitra and P. N. Sen, Phys. Rev. B **45**, 143 (1992).
[7] P. P. Mitra, P. N. Sen, L. M. Schwartz, and P. LeDoussal, Phys. Rev. Lett. **65**, 3555 (1992).
[8] Partha P. Mitra and Pabitra N. Sen, Physica A **186**, 109 (1992).
[9] P. P. Mitra, P. N. Sen, and L. M. Schwartz, Phys. Rev. B **47**, 8565 (1993).
[10] P. N. Sen, P. A. Goode, and A. Sibbit, J. Appl. Phys. **63**, 4832 (1988); L. M. Schwartz, P. N. Sen, and D. L. Johnson, Phys. Rev. B **40**, 2450 (1989).
[11] S. Frey, J. Kärger, H. Pfeifer, and P. Walther, J. Magn. Reson. **79**, 336 (1988).
[12] K. Fukuda, T. T. Kasuga, T. Mizusaki, A. Hirai, and K. Eguchi, J. Phys. Soc. Jpn. **58**, 1662 (1989).
[13] F. D'Orazio, S. Bhattacharja, W. P. Halperin, and R. Gerhardt, Phys. Rev. B **42**, 6503 (1990).
[14] R. M. Cotts, M. J. R. Hoch, T. Sun, and J. T. Marker, J. Magn. Reson. **83**, 252 (1989).
[15] D. L. Johnson, J. Koplick, and L. M. Schwartz, Phys. Rev. Lett. **57**, 2564 (1986).
[16] D. L. Johnson and P. N. Sen, Phys. Rev. B **24**, 2486 (1981); R. J. S. Brown, Geophysics **45**, 1269 (1980).
[17] W. Kenyon, J. Howard, A. Sezginer, C. Straley, A. Mat-

teson, K. Horkowitz, and R. E. Ehrlich, Paper LL, Trans. SPWLA Annu. Logging Symp. Volume II (1989).

[18]If the normal mode spectrum is discrete, the Green's function can be written as

$$G_0(\mathbf{r},\mathbf{r}',t) = \sum_{n=1}^{\infty} \psi_n(\mathbf{r})\psi_n(\mathbf{r}')e^{-E_n t} \ ,$$

where the eigenfunctions $\{\psi_n(\mathbf{r})\}$ form a complete orthonormal set. Because the lowest mode is constant in the pore space, the integrations over $\mathbf{r}$ and $\mathbf{r}''$ in (15b) lead immediately to the result $\mathcal{S}(t) = S$.

[19]L. M. Schwartz and D. L. Johnson, Phys. Rev. B **30**, 4302 (1984).

[20]K. R. Brownstein and C. E. Tarr, Phys. Rev. A **19**, 2446 (1979).

[21]P. N. Sen, C. Scala, and M. H. Cohen, Geophysics **46**, 781 (1981).

[22]J. Callaway, *Quantum Theory of the Solid State* (Academic, New York, 1976), Chap. 4.

[23]J. R. Banavar and L. M. Schwartz, in *Molecular Dynamics in Restricted Geometries,* edited by J. Klafter and J. M. Drake (Wiley, New York, 1989, p. 273; Phys. Rev. Lett. **58**, 1411 (1987).

[24]K. S. Mendelson, Phys. Rev. B **41**, 562 (1990); D. J. Wilkinson, D. L. Johnson, and L. M. Schwartz, Phys. Rev. **44**, 4960 (1991).

[25]The choice $\rho b/D_0 = 0.35$ is well within the fast diffusion regime (Refs. 20 and 24). A typical pore diameter, $d_p \approx b/5$ and $\rho d_p/D_0 \approx 0.05 \ll 1$.

[26]The value of γ used in this calculation (0.05) is twice as large as the value employed in Figs. 5 and 6, while the step size, ϵ, is only half as large. Note, however, that in the present case the cube edge and the pore diameter are *equal*, and so the value $\rho b/D_0 = 1.0$ is no longer strictly in the fast diffusion regime.

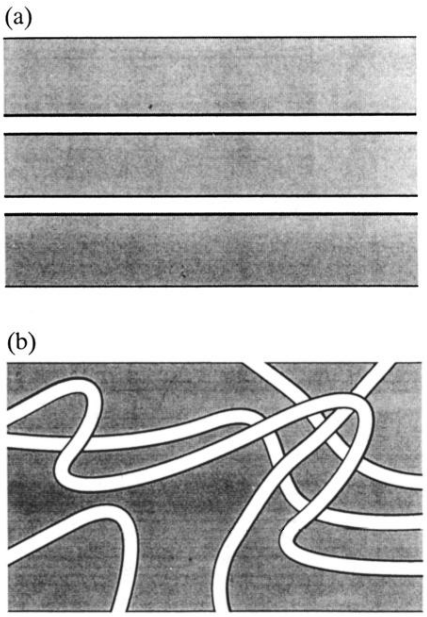

FIG. 1. (a) A pore space made of straight tubes. (b) A pore space comprised of a number of winding but nonintersecting tubes.

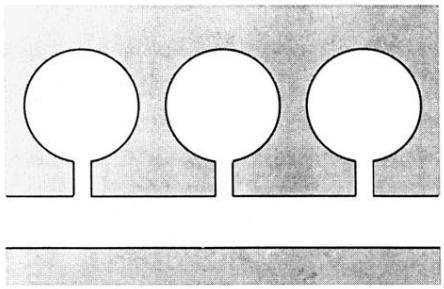

FIG. 2. A pore space made of straight tubes connected to "dead ends" by narrow throats.

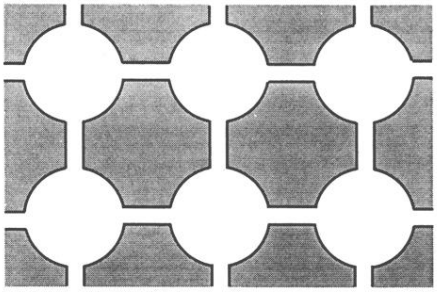

FIG. 3. A pore space comprised of large pores connected by narrow throats.

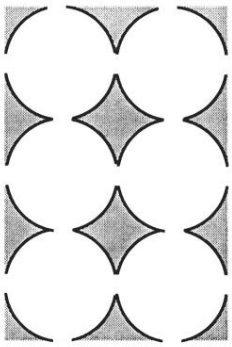

FIG. 4. A pore space in which the length of the connecting throats (shown in Fig. 3) has been decreased to zero while keeping the throat width constant.

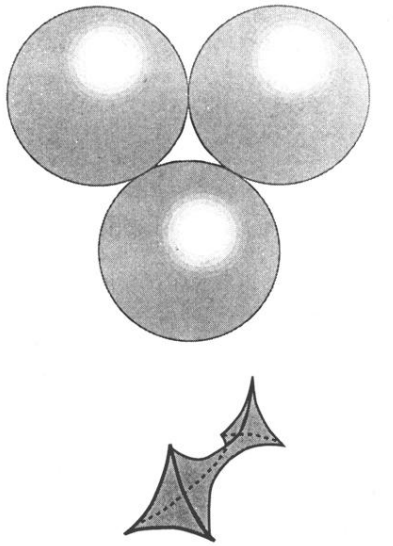

FIG. 8. Schematic representation of the throat formed by three touching spheres in a close packing environment. Throats of this kind are formed in a random packing with $\phi \approx 0.38$ and in a fcc packing with $\phi = 0.259$. The throats in a $\phi \approx 0.38$ fcc packing are formed by a similar configuration of *nonoverlapping* spheres.